Astron. Astrophys. 262, 37–48 (1992)

ASTRONOMY AND ASTROPHYSICS

# Time-resolved spectral analysis of three Seyfert galaxies observed with Ginga

**F. Fiore[1,2,⋆], G.C. Perola[1], M. Matsuoka[2], M. Yamauchi[2], and L. Piro[3]**

[1] Istituto Astronomico, Università di Roma "La Sapienza", via G.M. Lancisi, I-29 00161 Roma, Italy
[2] RIKEN, the Institute of Physical and Chemical Research, 2-1 Hirosawa, Wako, Saitama 351-01, Japan
[3] Istituto di Astrofisica Spaziale, C.N.R., C.P. 67, I-00044 Frascati, Italy

Received March 16, 1991; accepted February 8, 1992

**Abstract.** Observations by *Ginga* of bright Seyfert galaxies have revealed in their spectra the presence of a hard X-ray component which is probably produced, along with the iron K fluorescence line, by reprocessing of the primary one in optically thick matter. This discovery suggests that spectral variability can arise if the primary and the reprocessed components do not vary simultaneously. We attempted to explain the spectral variations observed by *Ginga* in IC 4329A, MCG-6-30-15 and NGC 4051 in the framework of the two component model. The behaviour of the first two objects in the range 1.7–18 keV and that of the third one above 4 keV can be well reproduced by the two component model, with a constant slope of the primary continuum, and the differences found can arise from the different sizes of the reprocessing region in individual objects. In IC 4329A the variations in the reprocessed component lags behind those in the primary one more than three days. In MCG-6-30-15 the lag is longer than a few hours. In this source, however, the spectral variations could also be due to changes in the slope of the primary component which are correlated with the intensity, and in this case the time lag would reduce to less than 90 min. In NGC 4051 the modest spectral variations above 4 keV are consistent with nearly simultaneous variations in both components, a result strengthened by the evidence, significant at the 99% confidence level, of variations of the iron fluorescence line, which are correlated with those of the continuum down to time scales as short as a few thousand seconds. On the other hand, in this galaxy the two component model is able to reproduce adequately neither the low energy spectral shape nor its large variations. The two modifications of this model that we tested, namely the assumption of a partial covering absorber or of an unobscured soft component, were both successful. In both cases the effective $N_H$ appears to be inversely correlated with the source intensity, thus lending support to the case of a "warm absorber" in this galaxy.

**Key words:** galaxies: Seyfert – galaxies: nuclei of – X-ray: spectroscopy

*Send offprint requests to*: F. Fiore (first address above)
⋆ Present address: Harvard-Smithsonian Center for Astrophysics, Mail Stop 4, 60 Garden Street, Cambridge, MA 02138, USA

## 1. Introduction

Spectral variability above 1 keV is a rather common phenomenon in Seyfert galaxies (SG). In most cases it can be roughly described as a softening of the spectrum when the source brightens, even if there is often a scatter around this general trend. This trend has been interpreted either as due to intrinsic changes of the spectral index which are correlated with the intensity (3C 120, Halpern 1985; NGC 4151, Perola et al. 1986; Fiore et al. 1990; Yaqoob & Warwick 1991; NGC 7314, Turner 1987; NGC 5548, Branduardi-Raymont 1986; NGC 4051, Lawrence et al. 1985, hereafter LWPE; Matsuoka et al. 1990, hereafter MPYM; MCG 6-30-15, MPYM), or as due to changes in the opacity of the absorbing gas along the line of sight in response to variations of the ionizing flux, the so-called "warm absorber" model (NGC 4151, Yaqoob et al. 1989; MR 2251-178, Halpern 1984; Pan et al. 1990; MCG 6-30-15, Nandra et al. 1990, hereafter NPS). Yet another interpretation, which is the main task of this paper to investigate, is related to the existence of a hard component in the SG spectra, and has been recently shown to work in the case of NGC 5548 by Nandra et al. (1991), a paper which appeared when our own was being submitted.

In the last five years EXOSAT and *Ginga* observations have provided evidence for the existence of optically thick matter in the innermost region of SG, which can modify the emergent spectrum (e.g. Pounds et al. 1990). Particularly relevant for the study of spectral variations in the *Ginga* energy band is the newly discovered hard component detected in several SG (e.g. Pounds et al. 1990; Piro et al. 1990; MPYM). This component was theoretically predicted by Guilbert & Rees (1988) and Lightman & White (1988) and probably represents the fraction of the power law continuum reprocessed by optically thick gas in the surroundings of the central source. The same gas should produce, through fluorescence, an iron line at about 6.4 keV, which, in fact, is a common feature in SG spectra. The positive correlation between iron line and continuum down to time scales as short as a few hundred seconds in NGC 6814 (Kunieda et al. 1990) suggests that the fluorescent material is located very close to the central engine.

Spectral variability between about 2 keV and a few tens of keV, the energy band in which the *Ginga* satellite is sensitive,

could arise if the power law and the reprocessed component do not vary simultaneously, that is, if the size of the central source is smaller than that of the "reprocessing region". If this were the case, then it would be possible to investigate the spatial distribution of the thick gas by studying the temporal variations of both the iron line intensity and of the spectral shape at high energies. The variations of the latter, particularly in faint sources, can be conveniently investigated through a hardness ratio. If the reprocessed component stays constant while the intensity of the power law varies, we shall observe a smooth correlation between the hardness ratio and the intensity. More realistically, the temporal behaviour of the reprocessed component, being related to the size of the "reprocessing region", will be a smoothed and delayed version of that of the primary one. Therefore, in general we should observe also a scatter around the correlation. To investigate this possibility we performed a careful time resolved analysis of the *Ginga* data of three Seyfert galaxies, IC 4329A, MCG-6-30-15 and NGC 4051, which are known to exhibit significant spectral variations or a clear high energy tail.

In Sect. 2 we describe the observations performed with the Large Area Proportional Counter on *Ginga* (details on *Ginga* and on the LAC can be found in Makino et al. 1987, Turner et al. 1989 and Hayashida et al. 1989), in Sects. 3–5 we present and discuss the results of the time resolved analysis for each one of the three sources, and in Sect. 6 we draw our conclusions. In Appendix we discuss the systematic errors in the reproduction of the *Ginga* LAC background, which can affect a spectral analysis.

## 2. Ginga observations and data reduction

IC 4329A was observed from July 8 to 10, 1989. Background observations were performed on July 7 and 12 by pointing at the same blank field. Data of detector no. 7 have been excluded from our analysis because its gain changed during the observations.

MCG-6-30-15 was observed from September 9 to 10, 1987. A background observation was performed on September 8. Data of two detectors had to be rejected because they were illuminated by the Sun, while the others were in the shadow of a solar panel.

NGC 4051 was observed from May 13 to 16, 1988. Background was acquired on May 12 and 17 from two different blank fields. Since the gain of detector no. 7 changed during the observation, its data have been excluded from the analysis.

The background subtraction is a very delicate matter because of the high variability of both its intensity and spectrum. It is, therefore, of primary importance to evaluate the magnitude of possible systematic errors, which might significantly affect a spectral variability search in relatively weak sources; we analyzed carefully this issue and the results are described in the Appendix.

In general the behaviour of the background in the mid and top layers is quite different, due to different guard and anticoincidence conditions (Hayashida et al. 1989); furthermore, the signal-to-noise ratio of the two layers combined is worse than that of the top layer alone below $\sim 8$ keV, and therefore also at the energy of the iron line, a feature we are particularly interested in. For these reasons, in the present analysis counts from the two layers are *not* combined together. The results obtained with the mid-layer above 8 keV were always compatible with those of the top layer and in the following only the results from the latter are presented.

The strategy chosen to study the spectral variations is based on two steps. The first is an analysis of hardness ratios, computed in each satellite orbit, as a function of the count rate. The counts between 1.7 and 18 keV were split into three intervals: 1.7–3.5, 3.5–5.8, 8.1–18 keV, thus leaving out the spectral region affected by the iron fluorescence line and K-edge absorption. From the counts in these bands the soft colour (SC: $C(3.5\text{–}5.8\text{ keV})/C(1.7\text{–}3.5\text{ keV})$) and the hard colour (HC: $C(8.1\text{–}18\text{ keV})/C(3.5\text{–}5.8\text{ keV})$) ratios were computed, which are intended to represent the spectral hardness at low and high energies. The crossover point in SC is the energy below which photoelectric absorption, or the effect of a soft component, can strongly modify the emergent spectrum, while 8 keV is the energy above which the reprocessed component is effective in introducing a significant flattening.

As a second step, to quantify the changes in those spectral parameters which are likely to be responsible for the observed colour variations, a spectral fitting analysis was performed over the entire energy range, thus including also the iron features. With the count statistics available, the conventional criterion in estimating the errors on each free parameter (Lampton et al. 1976) led to results which are inconclusive when such parameters could be more than one: the errors are often so large that the hypothesis of constant value for the parameters under investigation can hardly be excluded. Therefore, to cope with the evidence of spectral variations found in the colour analysis we took a less conservative approach, i.e. we estimated the errors using the criterion for the "single interesting parameter". All the errors quoted in this paper represent the 68% confidence interval.

For each of the three sources in Table 1 we give the mean value of the count rate in the 1.7–18 keV energy band, $C_T$, and in the soft, medium, and hard energy bands.

## 3. IC 4329A

The 1.7–18 keV count rate $C_T$ varied by about 20% from the first to the third day of observations, as can be seen in Fig. 1. The continuum spectrum of this source shows a significant flattening towards the high energies (Piro et al. 1990), well described by the "reflection bump" of Lightman & White (1988). For this reason and for its brightness, in spite of the small dynamic range of the

**Table 1.** Mean count rates

| Source | 1.7–18 keV[a] ($C_T$) | 1.7–3.5 keV[a] | 3.5–5.8 keV[a] | 8.1–18 keV[a] |
|---|---|---|---|---|
| IC 4329A | 7.4 | 2.5 | 2.9 | 1.0 |
| MCG-6-30-15 | 2.5 | 0.85 | 0.97 | 0.36 |
| NGC 4051 | 1.0 | 0.34 | 0.39 | 0.14 |

[a] in cts $s^{-1}$ $det^{-1}$.

observed variations, this source is a good candidate for a spectral variability search.

The soft and hard colours relative to each satellite orbit are plotted in Fig. 2a, b as a functions of $C_T$. While SC is consistent with a constant value ($\chi^2_r = 0.88$), HC appears variable, being smaller when the flux is higher ($\chi^2_r = 2.81$ corresponding to 0.03% probability of a constant value).

Within each day $C_T$ was nearly constant and both SC and HC were also consistent with a constant value. Furthermore, thanks to the high count rate, the systematic errors are negligible also between 18 and 30 keV, as shown in the Appendix. For these reasons, we felt justified in combining together the spectra of each day and in extending the useful energy range up to 30 keV. In the colour–colour diagram of Fig. 2c the hard colour is the ratio between the counts in the 8–30 keV and the 3.5–5.8 keV energy bands. It is evident again that the largest variations are seen in the high energy part of the spectrum. This behaviour can be naturally explained by a variation of the relative normalization in a model with two components such as the model consisting of a power law and the reprocessed continuum. The following model was, therefore, tested against the pulse height spectra of each day:

$$F(E) = [C_\gamma E^{-\Gamma}(1 + rA(E, \Gamma)) + I_{Fe}]e^{-\sigma(E)N_H}. \quad (1)$$

Here $\Gamma$ is the spectral photon index, $N_H$ the absorbing column and $\sigma(E)$ the Morrison & Mc Cammon (1983) cross section for cold gas with solar abundances; $A(E, \Gamma)$ is the X-ray albedo of the optically thick gas, as described by Lightman & White (1988) and White et al. (1988); $r$ is the ratio between the reprocessed and the primary component; $I_{Fe}$ is the intensity of the cold fluorescent iron line at the redshifted energy.

The results of the fit with all the parameters free are given in Table 2, columns 2–7: no significant evidence of variations is found this way in any of the parameters $\Gamma$, $N_H$ and $r$. The diagrams in Fig. 2 suggest, however, that it is reasonable to assume as constant both $\Gamma$ and $N_H$, because changes of the spectral index should produce similar variations in SC and HC, while changes of the absorbing column should produce variations in SC. Moreover, since the host galaxy is seen edge-on (Disney 1973), it is not unlikely that most of the observed absorption takes place in its interstellar medium.

The results obtained by fixing $\Gamma$ and $N_H$ to their mean values of 1.94 and $3.5\,10^{21}$ cm$^{-2}$, are presented in Table 2, columns 8, 9. In column 10 the normalization of the reprocessed component, $C_{RC} = rC_\gamma$, is also given. There is now a significant evidence of day to day variations in $r$. Also $C_{RC}$ appears to vary, the probability of a constant value being 0.4%, and to decrease while the source intensity is increasing: this behaviour indicates that the reprocessing gas in this galaxy responds to variations of the primary component on time scales longer than the duration of the present

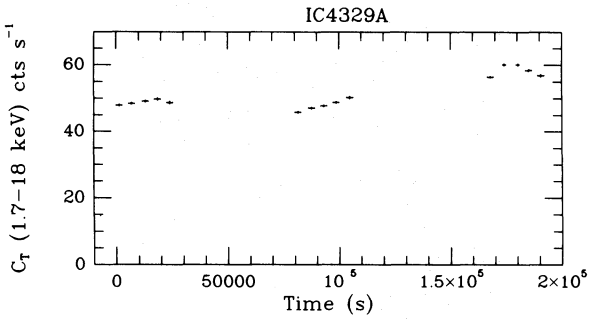


**Fig. 1.** IC 4329A: The light curve (seven detectors) in the 1.7–18 keV energy band. Each point represents one satellite orbit

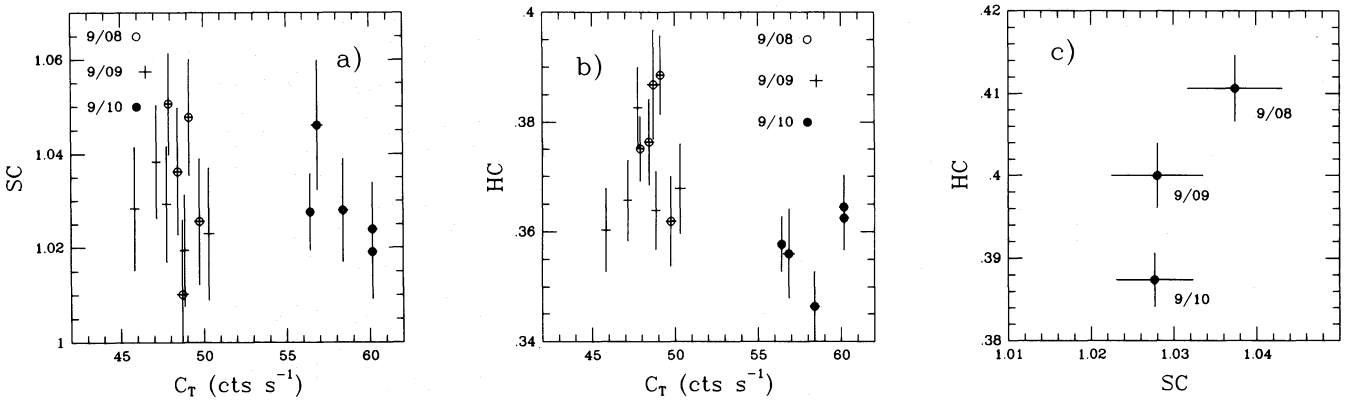


**Fig. 2a–c.** IC 4329A: **a** soft colour – intensity diagram, **b** hard colour – intensity diagram. Different symbols identify the three days of observation and each point represents one satellite orbit. **c** hard colour – soft colour diagram. Each point represents here the data collected in one day and HC is the $C$(8.1–30 keV)/$C$(3.5–5.8 keV) ratio

**Table 2.** IC 4329A, power law plus reprocessed component

| Day | $C_\gamma$[a] | $\Gamma$ | $N_H$[b] | $I_{Fe}$[c] | $r$ | $\chi^2_r(17)$ | $r$ | $\chi^2_r(19)$ | $C_{RC}$[a] |
|---|---|---|---|---|---|---|---|---|---|
| 7/08 | 42.6 | 1.919±0.041 | 3.6±0.7 | 14.2±2.0 | 1.32±0.35 | 0.74 | 1.53±0.07 | 0.77 | 66.2±3.2 |
| 7/09 | 43.1 | 1.944±0.043 | 3.7±0.7 | 12.7±2.0 | 1.35±0.38 | 0.64 | 1.31±0.07 | 0.58 | 56.3±3.1 |
| 7/10 | 53.4 | 1.949±0.032 | 3.4±0.6 | 16.4±2.0 | 1.11±0.26 | 1.16 | 0.97±0.06 | 1.15 | 51.3±3.1 |

[a] in units of $10^{-3}$ ph s$^{-1}$ cm$^{-2}$ keV$^{-1}$; [b] in units of $10^{21}$ cm$^{-2}$; [c] in units of $10^{-5}$ ph s$^{-1}$ cm$^{-2}$.

observation, namely three days. The other component representing the reprocessed radiation, the iron line, is not sufficiently constrained to check the above result: both its intensity and equivalent width are consistent with the constant values of $(1.44 \pm 0.12)\,10^{-4}$ ph s$^{-1}$ cm$^{-2}$ and $110 \pm 10$ eV, respectively.

## 4. MCG-6-30-15

The spectral shape and variability of MCG-6-30-15 have been analyzed and discussed by MPYM and NPS using the same *Ginga* observation treated in this paper. The two papers agree on two major results, the evidence of very thick gas and the detection of spectral variability, but they disagree on the interpretation of the latter: according to MPYM it can be attributed to variations of the spectral index correlated with the flux, while, according to NPS it is better described in terms of a "warm absorber" model where the power law continuum maintains a constant slope when varying in intensity. In both papers, however, the spectral variations are discussed in the framework of a model consisting of a simple power law plus low energy absorption. We shall further investigate this issue by taking into account the role possibly played by the reprocessed component. In the spectral fitting analysis we shall show that the soft excess component, discovered by Pounds et al. (1986) by using the EXOSAT LE telescope together with the ME proportional counters, did not significantly contribute to the emission above 1.7 keV.

The light curves in the soft, medium, high and 1.7–18 keV bands are shown in Fig. 3. During the 2 days of observations $C_T$ varied by up to a factor 2 on the time scale of hours. Within the exposure time along single satellite orbits, typically 20 out of 90 min, the variations in $C_T$ were confined to at most 30%, and we have found no significant evidence of changes in SC or HC within each one of the 17 orbits. On the contrary, when the two colours are estimated orbit-by-orbit, as they are plotted in Fig. 4a, b, they are both inconsistent with a constant value, namely this hypothesis can be excluded at the 99.98% ($\chi^2_r = 2.72$) confidence level for

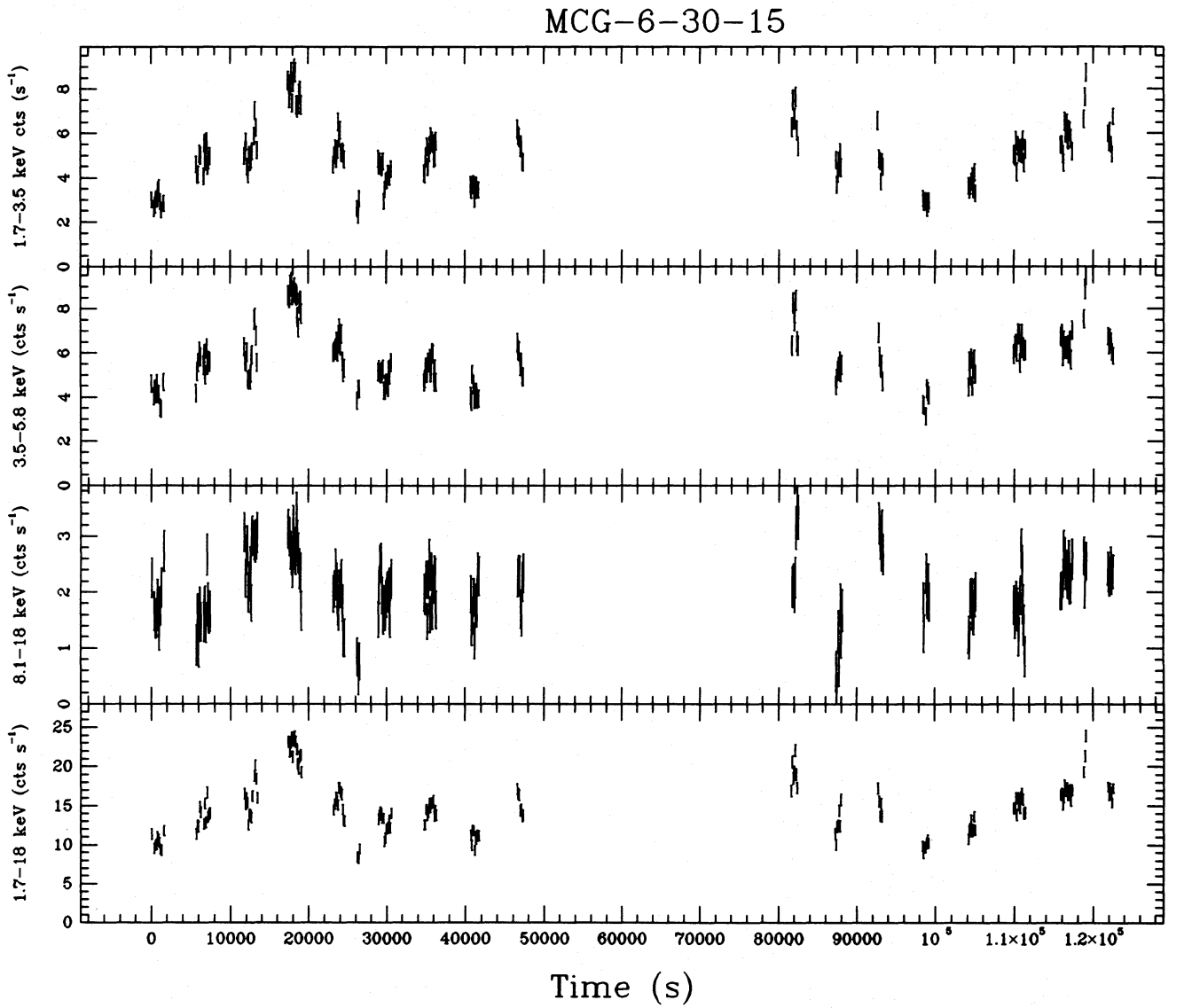


**Fig. 3.** MCG-6-30-15: The light curves (six detectors) in bins of 128 s: (a) 1.7–3.5 keV; (b) 3.5–5.8 keV; (c) 8.1–18 keV; (d) 1.7–18 keV ($C_T$)

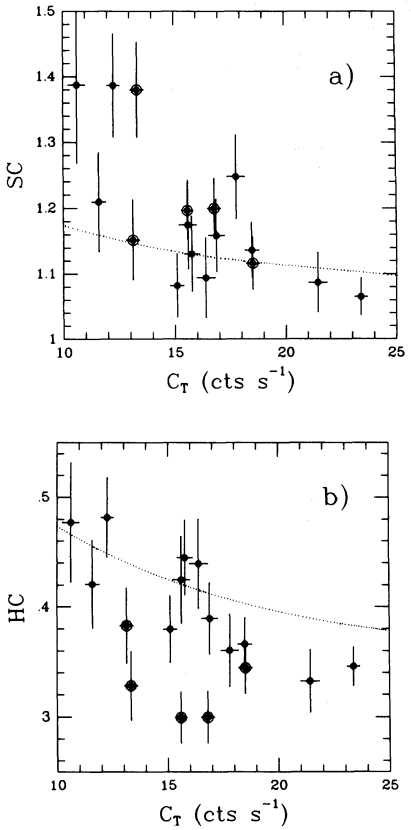


**Fig. 4a and b.** MCG-6-30-15: a) Soft Colour–Intensity diagram, b) Hard Colour–Intensity diagram. Each point represents one satellite orbit. The circles indicate the orbits probably affected by large systematic errors (see Sect. 4). The dotted lines represent the expectation when $\Gamma = 1.9$, $N_H = 7.5\,10^{21}$ cm$^{-2}$ and $C_{RC}$ constant with mean $r = 1.9$

SC and 99.99% ($\chi_r^2 = 3.06$) level for HC. Their behaviour with $C_T$ appears, however, different. In a linear regression analysis $\chi_r^2$ for SC becomes 1.49, with an improvement significant at the 99.99% confidence level ($F$-test, Bevington 1968), while $\chi_r^2$ for HC becomes 2.75, without a significant improvement: the variations in SC appear to be dominated by a smooth trend, while those in HC by a scatter.

To investigate whether the variations in HC might be caused by systematic errors, we applied the statistical procedure described in Appendix, and found that, for errors equal to the "fiducial" values given there, this hypothesis can be excluded at the 99.7% confidence level. However, when we tried the fit of model (1) to the 17 pulse height spectra, we found the resulting $\chi_r^2$ to be quite acceptable in 12 of them, but larger than 1.4 in the other 5, a number which is about 2.5 times larger than expected on purely statistical grounds. These five spectra belong to orbits 5, 6, 14, 15 and 16: since the satellite position was the same in orbits 5 and 15, as well as in orbits 6 and 16, and because the background spectrum depends strongly on the satellite position (see Appendix and Hayashida et al. 1989), we suspect that systematic errors in the background subtraction might be the cause of this result. If, on these grounds, the five orbits (the circled points in Fig. 4) are excluded, as we shall conservatively do in the following, the situation with the scatter in HC changes radically. While the probability of a constant value remains low for both SC and HC, 0.3 and 0.6%, respectively, the linear regression analysis yields $\chi_r^2 = 1.46$ for SC and 0.75 for HC: the variations in both colours appear now to be dominated by a smooth inverse correlation with $C_T$.

To investigate the cause of this correlation in terms of the parameters $\Gamma$, $N_H$ and $r$ of model (1), we decided to optimize the signal-to-noise ratio by grouping the 12 orbits into three spectra in the following ranges of $C_T$, 10–14 cts s$^{-1}$ (spectrum L), 14–20 cts s$^{-1}$ (spectrum I), 20–25 cts s$^{-1}$ (spectrum H).

The errors from the fit to model (1) with the three parameters free are so large that each of them turns out consistent with a constant value. We therefore repeated the fit with either $r$ (*case A*), or $\Gamma$ (*case B*) held fixed. In *case A*, by fixing $r$, we are assuming that the two components vary simultaneously; we adopted $r = 2.2$, the mean value found by MPYM. In *case B* we fitted the spectra for a grid of $\Gamma$ values: the best results in terms of $\chi^2$ were obtained with $\Gamma$ in the range 1.8 to 2.0. The results are given in Table 3 for *case A*, and in Table 4 for *case B* with $\Gamma = 1.9$. The $\chi_r^2$ values are quite

**Table 3.** MCG-6-30-15, power law plus reprocessed component, $r = 2.2$ fixed

| | $C_\gamma$[a] | $\Gamma$ | $N_H$[b] | $I_{Fe}$[c] | $C_{RC}$[a] | $EW_{RC}$[d] | $\chi_r^2(17)$ |
|---|---|---|---|---|---|---|---|
| L | 7.9 | $1.676 \pm 0.062$ | $7.2 \pm 2.8$ | $13.0 \pm 3.7$ | $17.3 \pm 2.2$ | $2.08 \pm 0.66$ | 1.21 |
| I | 14.3 | $1.841 \pm 0.036$ | $5.8 \pm 1.5$ | $11.7 \pm 2.7$ | $31.4 \pm 2.2$ | $1.40 \pm 0.34$ | 0.78 |
| H | 29.2 | $2.066 \pm 0.047$ | $10.0 \pm 1.7$ | $4.3 \pm {}^{4.6}_{4.3}$ | $64.2 \pm 5.6$ | $0.38 \pm {}^{0.42}_{0.38}$ | 1.03 |

[a] in units of $10^{-3}$ ph s$^{-1}$ cm$^{-2}$ keV$^{-1}$; [b] in units of $10^{21}$ cm$^{-2}$; [c] in units of $10^{-5}$ ph s$^{-1}$ cm$^{-2}$; [d] in keV.

**Table 4.** MCG-6-30-15, power law plus reprocessed component, $\Gamma = 1.9$ fixed

| | $C_\gamma$[a] | $N_H$[b] | $I_{Fe}$[c] | $r$ | $C_{RC}$[a] | $EW_{RC}$[d] | $\chi_r^2(17)$ |
|---|---|---|---|---|---|---|---|
| L | 10.3 | $10.5 \pm 2.3$ | $12.0 \pm 3.7$ | $4.8 \pm 0.9$ | $49.6 \pm 9.6$ | $1.02 \pm 0.45$ | 1.24 |
| I | 15.3 | $6.7 \pm 1.1$ | $11.3 \pm 2.7$ | $2.8 \pm 0.4$ | $43.6 \pm 6.2$ | $1.09 \pm 0.30$ | 0.78 |
| H | 23.7 | $7.5 \pm 1.2$ | $5.0 \pm 4.7$ | $0.6 \pm 0.4$ | $14.2 \pm 9.5$ | $1.5 \pm {}^{1.7}_{1.5}$ | 0.94 |

[a] in units of $10^{-3}$ ph s$^{-1}$ cm$^{-2}$ keV$^{-1}$; [b] in units of $10^{21}$ cm$^{-2}$; [c] in units of $10^{-5}$ ph s$^{-1}$ cm$^{-2}$; [d] in keV.

acceptable for each one of the three spectra and equally good for *case A* and *case B*. In Fig. 5 a representative example of the residuals is given: it is apparent that the addition to model (1) of one more component, representing a tail above 1.7 keV of the soft excess detected with EXOSAT (Pounds et al. 1986; Nandra et al. 1989), is not required by these data.

Let us now comment on the behaviour of the free parameters. Concerning $N_H$, there is no significant evidence of variations both with $r$ or $\Gamma$ fixed: its mean value is approximately the same in the two instances, namely $7.5\,10^{21}$ cm$^{-2}$, and the constant hypothesis test yields a probability of 18% (*case A*) and of 33% (*case B*). Contrary to NPS, we therefore find no supporting evidence, in terms of an anticorrelation between $N_H$ and $C_T$, for the presence of a "warm absorber" in this observation.

In *case A* the spectral index varies significantly (the probability of a constant value is $10^{-6}$), and the MPYM result on the existence of a correlation between $\Gamma$ and the unabsorbed flux $F^c$ in the band 2–10 keV is recovered. Quantitatively, we find $\Gamma=(1.32\pm0.12)+(0.11\pm0.021)F^c$.

In *case B* the quantity $r$ varies significantly (the probability of a constant value is $2\,10^{-6}$) and in opposite direction with respect to the intensity of the primary spectral component (represented in Table 4 by $C_\gamma$). Qualitatively, this behaviour is consistent with a constant intensity of the reprocessed component (represented in Table 4 by $C_{RC}=rC_\gamma$). Quantitatively, however, $C_{RC}$ is compatible with a constant value only at the 1.4% confidence level, and its best fit value indicates a decrease in correspondence to the increase of $C_\gamma$. Since the three spectra were obtained by summing orbits according to their flux level but with no regard to their temporal ordering, this indication implies that the variations in $C_{RC}$ should have occurred in opposition to the large amplitude variations in the primary component: from an inspection of the light curve in Fig. 3, the variations in $C_{RC}$ should have responded to those in $C_\gamma$ with a delay of the order of 15 000 s. Notably, if this were the case, the trend in the colours should be steeper than predicted with a constant $C_{RC}$. In Fig. 4 the trend expected with $C_{RC}$ equal to the mean value obtained from the fits, namely $3.8\,10^{-2}$ cm$^{-2}$ s$^{-1}$ keV$^{-1}$, is shown and is indeed shallower than observed, the agreement being acceptable only at the 6 and 4% confidence levels for SC and HC, respectively.

Under the assumption of a constant slope in the primary component, we would then conclude that there is some evidence, from spectral fitting and colour analyses, that the reprocessed component responds to variations in the primary one with a lag longer than one orbit and shorter than the observation. Further insight on the existence of such a lag could in principle be obtained directly from a cross-correlation analysis of the continua at low energies, where the contribution of the reprocessed component is negligible, and at high energies: with respect to the auto-correlation function at low energies, a shift towards positive values of the lag should be evident in the cross-correlation function. We therefore estimated the cross-correlation function of the continua in the bands 1.7–3.5 and 8.1–18 keV, and the auto-correlation function in the first band, using the algorithm of Edelson & Krolik (1988) for nonequispaced data. The results are shown in Fig. 6: unfortunately, given the errors on the coefficients, it is apparent that no significant conclusion can be drawn from a comparison between the two correlations.

Concerning the last free parameter in our fits, the intensity of the iron line has practically identical values in *case A* and *case B* (Table 3, Column 5; Table 4, Column 4), and is consistent with a constant value (44% probability). Its average equivalent width is $EW=210\pm40$ eV. If it is assumed that the bulk of the line comes from the same gas responsible for the reprocessed continuum, the results obtained in the two cases can be tested for consistency with this assumption by using the equivalent width $EW_{RC}$ of the line with respect to the reprocessed continuum (Tables 3 and 4, Column 7), which should stay constant in time. This analysis leads to the interesting result that, while in *case B* $EW_{RC}$ is consistent with a constant value at the 96% confidence level, in *case A* the same is true only at the 5% level.

In conclusion, the present data on MCG-6-30-15 are consistent with model (1). However, with the statistics available, it is hardly possible to discriminate between variations in the slope $\Gamma$ of the primary spectral component, and in the ratio $r$ between the reprocessed and primary components, as the main cause of the observed anticorrelation between the colours and the count rate; as we have just shown, the only marginal evidence in favour of the second instance is found in the behaviour of the iron line.

## 5. NGC 4051

The X-ray spectral variability of this source has so far been studied by LWPE and by MPYM. The former authors, using the

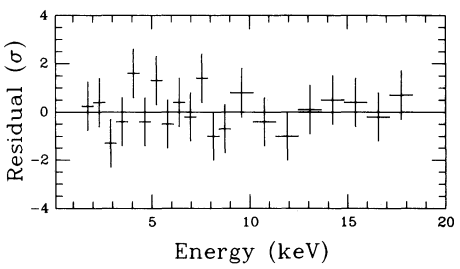


**Fig. 5.** The residuals after subtracting from the PHA spectrum of MCG-6-30-15 at intermediate flux level (I) the best fit with model (1) with $\Gamma$ fixed at 1.9

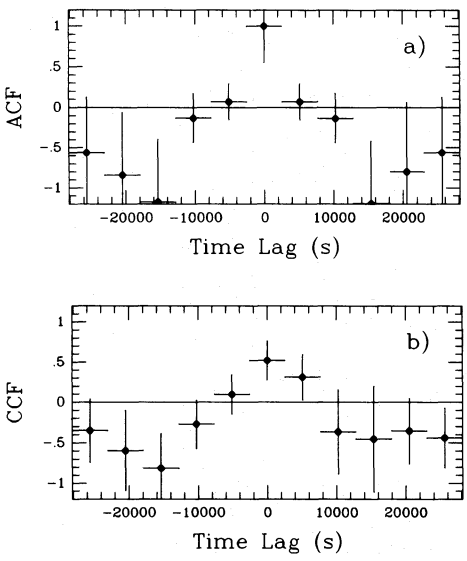


**Fig. 6a and b.** MCG-6-30-15: **a** the auto-correlation function of the light curve in the 1.7–3.5 keV energy band; **b** the cross-correlation function of the light curves in the bands 1.7–3.5 and 8.1–18 keV. Each point represents the mean correlation in 5120 s.

LE telescope (0.1–2 keV) and the ME proportional counters (1–10 keV) on board of EXOSAT, discovered a systematic change of the 0.1–10 keV spectral shape that became steeper during the brightest episodes. They attributed this effect either to a change of the LE + ME spectral index or to the additional contribution of a soft component which dominates the LE count rate. The very thin absorbing column derived by fitting the LE+ME data to a simple power law, lower than the galactic value along the line of sight, and the imperfect correlation between the LE and ME light curves were regarded as evidence of the existence of two distinct components below 2 keV.

MPYM found similar spectral variations in a *Ginga* observation performed on June 1987. They attributed these spectral variations to a change in the spectral index, which can be quantified in $\Delta\alpha \sim 0.5$ for a factor four variation in the 2–20 keV flux.

Here we present the results of a second *Ginga* observation and show that the high energy behaviour of this source is compatible with the model adopted for the two previous sources. Its low energy variations, however, require additional hypotheses. Results from this observation have been published by Done et al. (1990) as a part of a simultaneous multifrequency campaign. A spectral analysis of this observation has also been performed by Kunieda et al. (1991).

The light curves in the soft, medium, hard and 1.7–18 keV energy bands are plotted in bins of 256 s in Fig. 7. Variations up to a factor ~4–5 are present on the time scale of hours, as well as changes of smaller amplitude on shorter time scales. To the effect of studying the spectral variability the fact that the count rate $C_T$(1.7–18 keV) was on average two times smaller than in MCG-6-30-15, is compensated by its dynamic range being two times larger.

The soft and hard colours are plotted against $C_T$ in Fig. 8a, b. The two diagrams look quite different. SC is clearly not constant (the corresponding probability is $4\,10^{-12}$) and shows both an inverse trend with the flux (the correlation coefficient is −0.68,

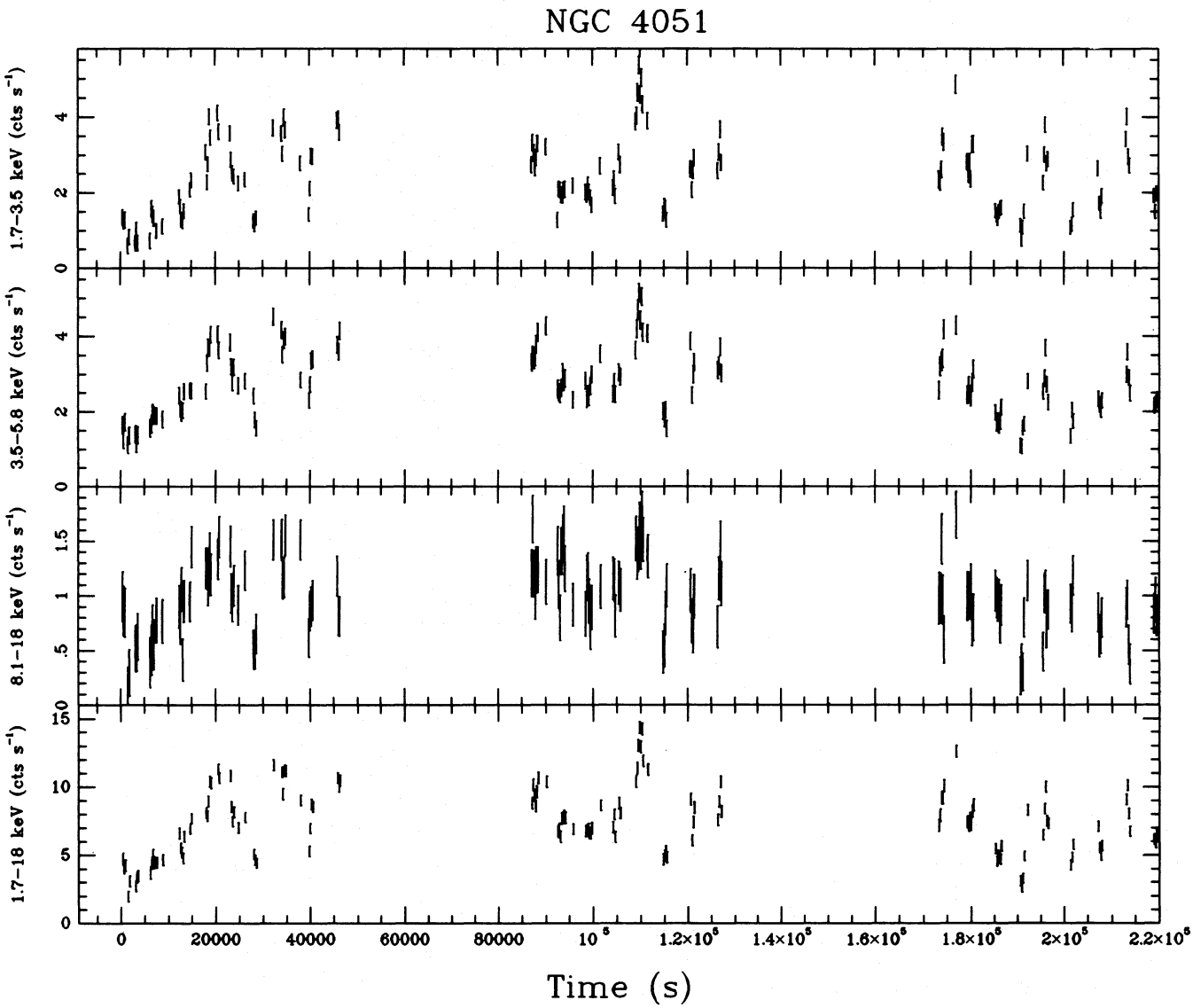


**Fig. 7.** NGC 4051: The light curves (seven detectors) in bins of 256 s: (a) 1.7–3.5 keV; (b) 3.5–5.8 keV; (c) 8.1–18 keV; (d) 1.7–18 keV ($C_T$)

**Table 5.** NGC 4051, power law with uniform absorber, 1.7–10 keV

| | $C^a$ | $\Gamma$ | $N_H{}^b$ | $I_{Fe}{}^c$ | $\chi^2_r(10)$ |
|---|---|---|---|---|---|
| L7 | 4.4 | $1.60\pm0.09$ | $10.2\pm3.4$ | $1.5\pm1.4$ | 1.08 |
| I3H | 7.4 | $1.84\pm0.08$ | $15.0\pm2.8$ | $4.9\pm1.9$ | 1.85 |
| I6 | 7.6 | $1.78\pm0.06$ | $5.4\pm1.9$ | $3.5\pm1.4$ | 1.76 |
| I4S | 7.4 | $1.83\pm0.04$ | $0+3.5$ | $4.4\pm1.8$ | 1.49 |
| H4 | 10.4 | $1.85\pm0.06$ | $4.3\pm1.8$ | $5.7\pm1.9$ | 0.75 |

[a] 1.7–10 keV cts $s^{-1}$ for 7 detectors; [b] in units of $10^{21}$ $cm^{-2}$; [c] in units of $10^{-5}$ ph $s^{-1}$ $cm^{-2}$.

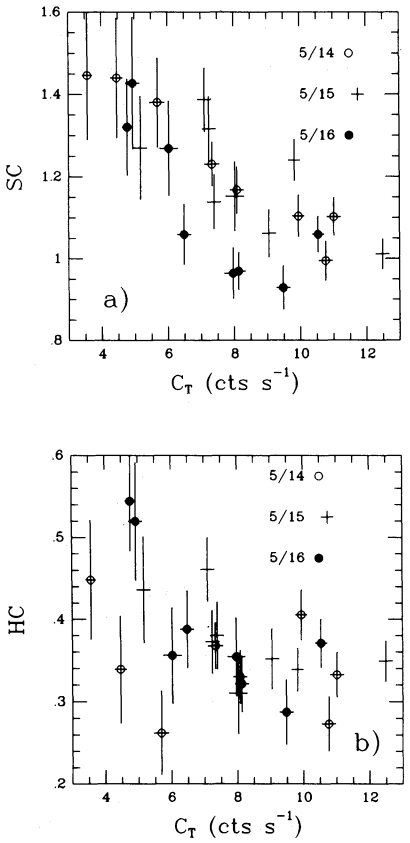


**Fig. 8a and b.** NGC 4051: **a** soft colour–intensity diagram, **b** hard colour–intensity diagram. Each point represents one satellite orbit. Different symbols identify the three days of observation

corresponding to a probability of 99.98%), and a large scatter around it (the $\chi^2_r$ of a linear correlation is 3.19). It is important to remark that the systematic errors in the background subtraction have little influence on the SC values. On the other hand, given a correlation between SC and the intensity, and the fact that the latter varies by up to a factor 1.5 also on time scales shorter than the single orbit exposure time, as clear from Fig. 7, the deviations from a linear trend in the SC diagram could be determined by differences in the light curves within orbits with approximately the same mean count rate. To investigate if this were the case, the colours were also computed by using the data in bins of 256 s: the scatter in SC remains and is determined mainly by the low value of points belonging to the third day of observation. In fact, the $\chi^2_r$ of a linear correlation reduces to 1.49 (11% probability) when the points belonging to the third day are excluded.

The $\chi^2_r$ for a constant HC is 2.03 (corresponding to a probablity of $2.5\,10^{-3}$). However, the variance in HC is comparable to that expected from the systematic errors estimated in the Appendix. Therefore, the hypothesis of a nearly constant HC cannot be excluded. The behaviour of the colours indicates that most of the action leading to spectral variations in this galaxy takes place at energies below 10 keV. This indication will be confirmed by the spectral fitting.

To optimize the signal-to-noise ratio we added together spectra of different orbits with similar values of SC, in order to avoid at our best the mixing of spectra with similar $C_T$ but evidently different spectral parameters. This problem is particularly evident in Fig. 8a at intermediate flux levels ($6 \le C_T \le 10$ cts $s^{-1}$). In this interval of flux we grouped together the four points of the third day with SC $\le 1.06$ (spectrum I4S), the three points of the second day with SC $\ge 1.24$ (spectrum I3H) and the remaining 6 points ($1.06 \le$ SC $\le 1.24$, spectrum I6); we then grouped together the seven points with the lowest and the four with the highest flux (spectra L7 and H4). We would like to remark that this subdivision preserves a sort of temporal resolution at intermediate flux levels, which can allow one to obtain information on the nature of the variations responsible for the SC scatter. Furthermore, the SC correlation with $C_T$ can be investigated by using only the spectra, L7, I6 and H4, thus avoiding the complications induced by the scatter.

The fit of model (1) to the five spectra over the energy range 1.7–18 keV leads to very unstable and practically insignificant results on $\Gamma$ and $r$, which are likely to be caused by the strong correlation between these two parameters in addition to the limited statistics above 10 keV; furthermore, the $\chi^2$ for the spectra I3H and I4S is not satisfying. First, to avoid the former complication we fitted this model over the restricted energy range 1.7–10 keV without the reprocessed continuum ($r=0$), to obtain the results given in Table 5. The $\chi^2_r$ for the spectra I3H, I6 and I4S is unacceptably large. The poor quality of the fit is illustrated in Fig. 9 for the spectrum I6 taken as an example: the behaviour of the residuals indicates that the model should be modified at low energies.

The first modification of model (1) was the assumption of an inhomogeneous, partial covering (PC) absorber: it consists in introducing one further parameter, $F_C$, representing the covered fraction of the source:

$$F(E)=\{C_\gamma E^{-\Gamma}[1-F_C+F_C e^{-\sigma(E)N_H}] \times [1+rA(E,\Gamma)]+I_{Fe}\}e^{-\sigma(E)N_{Hg}}, \quad (2)$$

where $N_{Hg}$ is the galactic value along the line of sight equal to $1.1\,10^{20}$ $cm^{-2}$.

We fitted first the spectra in the range 1.7–10 keV with $r=0$ to obtain the results given in Table 6. The $\chi^2_r$ for the spectra I3H, I6 and I4S is substantially improved and are now fully acceptable; notably, the spectral index turns out to be consistent with a constant value, and we therefore fitted the model over the full range 1.7–18 keV with $\Gamma$ fixed at the average value obtained, namely $\Gamma=2.1$, but now with $r$ as a free parameter. The results are listed in Table 7 (columns 3–8), where also those obtained over the same energy range with $r=0$ are given (columns 9–12). The improvement in the $\chi^2$ values when the reprocessed continuum is

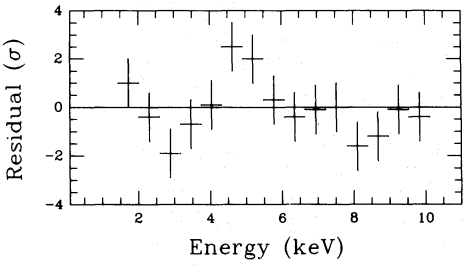


**Fig. 9.** The residuals after subtracting from the PHA spectrum of NGC 4051 at intermediate flux level (I6) the best fit with model (1) with $r=0$ over the band 1.7–10 keV

**Table 8.** NGC 4051, power law plus thermal bremsstrahlung (kT = 0.7 keV), 1.7–10 keV

| | $\Gamma$ | $N_H$[a] | $C_{TB}$[b] | $I_{Fe}$[c] | $\chi^2_r(10)$ |
|---|---|---|---|---|---|
| L7 | $1.89\pm0.14$ | $4.3\pm1.2$ | $6.2\pm1.6$ | $0.7\pm^{1.5}_{0.7}$ | 0.49 |
| I3H | $2.15\pm0.11$ | $4.8\pm0.9$ | $10.4\pm1.9$ | $4.0\pm2.0$ | 0.87 |
| I6 | $2.04\pm0.09$ | $3.6\pm0.8$ | $12.9\pm2.3$ | $2.5\pm1.5$ | 1.13 |
| I4S | $1.99\pm0.13$ | $2.9\pm1.2$ | $15.9\pm^{2.9}_{4.1}$ | $3.4\pm2.0$ | 1.13 |
| H4 | $1.93\pm0.11$ | $1.6\pm^{0.7}_{1.2}$ | $9.4\pm^{4.0}_{9.4}$ | $5.4\pm2.0$ | 0.74 |

[a] in units of $10^{22}$ cm$^{-2}$; [b] in units of $10^{-3}$ ph s$^{-1}$ cm$^{-2}$ keV$^{-1}$; [c] in units of $10^{-5}$ ph s$^{-1}$ cm$^{-2}$.

**Table 6.** NGC 4051, power law with partial covering, 1.7–10 keV

| | $\Gamma$ | $N_H$[a] | $F_C$ | $I_{Fe}$[b] | $\chi^2_r(18)$ |
|---|---|---|---|---|---|
| L7 | $1.93\pm0.17$ | $9.0\pm3.0$ | $0.58\pm0.07$ | $0.4\pm^{1.6}_{0.4}$ | 0.54 |
| I3H | $2.19\pm0.14$ | $8.4\pm1.6$ | $0.67\pm0.05$ | $3.4\pm1.9$ | 0.87 |
| I6 | $2.15\pm0.15$ | $11.5\pm2.0$ | $0.52\pm0.06$ | $1.6\pm1.6$ | 0.53 |
| I4S | $2.21\pm0.14$ | $22.0\pm6.0$ | $0.44\pm^{0.10}_{0.16}$ | $1.9\pm1.9$ | 1.03 |
| H4 | $1.92\pm0.10$ | $4.5\pm2.6$ | $0.28\pm^{0.09}_{0.11}$ | $5.3\pm1.9$ | 0.74 |

[a] in units of $10^{22}$ cm$^{-2}$; [b] in units of $10^{-5}$ ph s$^{-1}$ cm$^{-2}$.

included is significant at the 98, 99.5 and 99% confidence level for the spectra I3H, I6 and H4, respectively.

Concerning $N_H$ and $F_C$, only the variations in $F_C$ are highly significant (at the 99.98% level). $N_H$ is consistent with a constant, but we note that its value for the spectrum I4S is larger than the mean at the 90% level of significance. If we take the product $N_H \times F_C$ as an estimate of the effective absorption, the hypothesis of an inverse correlation with $C_T$ is significant at the 97% level, and the improvement in $\chi^2$ with respect to the constant hypothesis is significant at the 99.9% level. This result indicates that the cause of the trend in SC versus $C_T$ might be the ionization of the absorber by the continuum ("warm absorber"). The scatter around the trend could be due to structural changes in the absorber occurring on the time scale of one day or less, as suggested by the above noted marginally significant discrepancy between the mean $N_H$ and its value in the spectrum I4S.

The second modification of model (1) consists in the addition of a soft component, which accounts for the evidence of an excess in the 0.1–2 keV band claimed by LWPE, which might be important also at energies somewhat higher than 2 keV. As suggested by a physical model proposed by Courvoisier & Camenzind (1989) and by Walter & Courvoisier (1990), we assumed this component to be clear of the gas absorbing the hard component. The excess was parametrized as a thermal bremsstrahlung. The only useful result from the fit with all the parameters free was the range 0.3 to 0.7 keV for the acceptable values of the temperature. We then fitted the spectra in the range 1.7–10 keV with $r=0$ and with $kT$ fixed at values within the above range in steps of 0.1 keV. The values of the other parameters are practically insensitive to the temperature adopted; the results reported in Table 8 are those relative to $kT=0.7$.

The spectral index turns out again consistent with a constant value and, therefore, we extended the analysis to the entire energy range with $\Gamma$ fixed at the average value of 2.1 obtained from the previous fit, including the reprocessed component. The results are given in Table 9. The spectral changes now appear to be due to combined variations of $N_H$ and of the normalization $C_{TB}$ of the soft component. $N_H$ is anticorrelated with the flux (the improvement in $\chi^2$ with respect to the constant hypothesis is significant at the 99.9% level), as one would expect if the absorber were "warm". On the other hand, the variations of $C_{TB}$ seems to be responsible for the scatter in the SC diagram.

In both modifications the fit to the data favours a "warm absorber", and we would then conclude that photoionization of the absorber by the incident continuum is probably the cause of the trend in SC versus $C_T$, while the cause of its scatter could be due to rather fast ($\leq 1$ day) changes either in the configuration of the absorber itself or in the soft component.

With regard to the reprocessed component, we note that in both modifications of model (1) the quantity $r$ appears to be consistent with the constant value of $1.9\pm0.4$, while the iron line intensity in the high flux spectrum is about $2\sigma$ greater than that in

**Table 7.** NGC 4051, power law with partial covering plus reprocessed component

| | $C_T$[a] | $C_\gamma$[b] | $N_H$[c] | $F_C$ | $I_{Fe}$[d] | $r$ | $\chi^2_r(15)$ | $N_H$[c] | $F_C$ | $I_{Fe}$[d] | $\chi^2_r(16)$ |
|---|---|---|---|---|---|---|---|---|---|---|---|
| L7 | 4.8 | 7.4 | $8.7\pm2.2$ | $0.62\pm0.04$ | $0.0+1.4$ | $2.0\pm1.1$ | 0.48 | $12.2\pm1.7$ | $0.66\pm0.02$ | $0.0\pm1.8$ | 0.73 |
| I3H | 8.0 | 11.1 | $5.6\pm1.6$ | $0.62\pm0.06$ | $1.8\pm1.8$ | $2.3\pm0.9$ | 1.36 | $9.0\pm1.3$ | $0.64\pm0.03$ | $1.8\pm1.8$ | 1.87 |
| I6 | 8.2 | 10.7 | $7.9\pm2.4$ | $0.42\pm0.03$ | $1.0\pm1.0$ | $2.0\pm0.8$ | 1.11 | $13.2\pm1.9$ | $0.51\pm0.02$ | $0.0+2.5$ | 1.87 |
| I4S | 7.8 | 11.3 | $20.2\pm8.3$ | $0.33\pm0.12$ | $2.0\pm2.0$ | $0.7\pm^{1.4}_{0.7}$ | 1.06 | $23.6\pm5.7$ | $0.39\pm0.04$ | $1.5\pm^{1.8}_{1.5}$ | 1.02 |
| H4 | 11.0 | 13.2 | $3.6\pm^{2.6}_{2.2}$ | $0.40\pm^{0.23}_{0.07}$ | $4.8\pm1.9$ | $1.8\pm0.7$ | 0.96 | $8.8\pm2.1$ | $0.41\pm0.03$ | $4.5\pm1.9$ | 1.43 |

[a] 1.7–18 keV cts s$^{-1}$ for 7 detectors, [b] in units of $10^{-3}$ ph s$^{-1}$ cm$^{-2}$ keV$^{-1}$; [c] in units of $10^{22}$ cm$^{-2}$; [d] in units of $10^{-5}$ ph s$^{-1}$ cm$^{-2}$.

**Table 9.** NGC 4051, power law plus thermal bremsstrahlung ($kT=0.7$ keV) plus reprocessed component

| | $C_\gamma$[a] | $N_H$[b] | $C_{TB}$[a] | $I_{Fe}$[c] | $r$ | $\chi^2_r(15)$ |
|---|---|---|---|---|---|---|
| L7 | 7.2 | $4.8\pm0.8$ | $6.5\pm1.4$ | $0.0\pm1.4$ | $2.2\pm1.0$ | 0.45 |
| I3H | 11.1 | $3.6\pm0.7$ | $8.1\pm2.5$ | $1.9\pm1.9$ | $2.2\pm0.8$ | 1.34 |
| I6 | 10.7 | $3.1\pm0.6$ | $11.2\pm2.5$ | $1.2\pm1.2$ | $2.1\pm0.7$ | 1.14 |
| I4S | 9.9 | $3.0\pm0.9$ | $15.9\pm3.7$ | $2.6\pm2.0$ | $1.5\pm0.9$ | 1.04 |
| H4 | 13.4 | $1.8\pm^{0.6}_{0.8}$ | $9.3\pm^{4.5}_{7.2}$ | $4.8\pm1.9$ | $1.7\pm0.7$ | 0.96 |

[a] in units of $10^{-3}$ ph s$^{-1}$ cm$^{-2}$ keV$^{-1}$; [b] in units of $10^{22}$ cm$^{-2}$; [c] in units of $10^{-5}$ ph s$^{-1}$ cm$^{-2}$.

the low flux spectrum. To further investigate the correlation between line and continuum, we computed the line flux from the spectra accumulated every 256 s. The line count rate was estimated by subtracting from the counts in a narrow interval centred at the line energy a continuum computed by interpolating the counts in two adjacent bands. In Fig. 10 the histogram represents the average counts in the line in three flux intervals. Here the errors represent the dispersion of the points in each flux interval. The mean count rate is equal to $0.14\pm0.02$ cts s$^{-1}$ (corresponding to an EW$=90\pm35$ eV) and the constant value hypothesis can be excluded at the 99% confidence level; the improvement in $\chi^2$ for a linear correlation is significant at the 97.5% confidence level.

The results on $r$ and $I_{Fe}$ consistently indicate that the reprocessed component in this galaxy responds very quickly to variations of the primary continuum. This conclusion is further strengthened by the results of a cross correlation analysis, carried out with the same technique used for MCG-6-30-15, which in this case are statistically significant. In Fig. 11a, b we give the cross correlation coefficients for the line and 3.5–5.8 keV continuum and for the two bands 3.5–5.8, 8.1–18 keV of the continuum; in both cases, the only coefficient significantly larger than zero is the one centred at zero lag, thus implying a response in the reprocessed component occurring with a lag of at most a few thousand seconds.

## 6. Conclusions

We have studied the X-ray spectral variability in *Ginga* observations of three SG, namely, in order of decreasing intensity and increasing amplitude of the detected intensity variations IC 4329A, MCG-6-30-15 and NGC 4051. Our goal was mainly to assess the impact on their spectral variations of the reprocessed component (RC) discovered with *Ginga* in several SG and to investigate the possibility of estimating the time lags in the response of RC to changes in the primary component (PC). The main conclusions can be summarized as follows:

(a) In the spectra of the three galaxies there is a clear evidence of an "excess" at high energies and of the iron fluorescence line at 6.4 keV, both of which can be regarded as signatures of RC.

(b) Spectral variations are present in all three galaxies, but those at high and low energies compare differently in each of them: in IC 4329A variations are evident only in the Hard Colour, in MCG-6-30-15 both in the Hard and Soft Colour, in NGC 4051 in the Soft Colour but only marginally in the Hard Colour.

(c) In all three sources the hypothesis of a constant slope in PC is statistically acceptable. Within the framework of the two component model, the behaviour of their continuum implies that

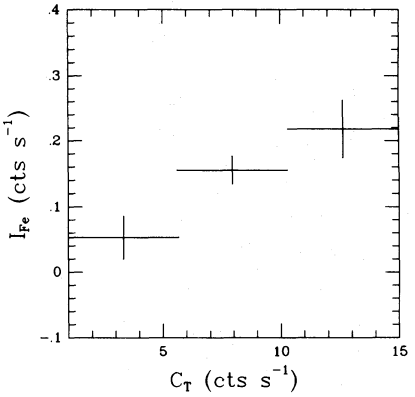


**Fig. 10.** NGC 4051: iron line counts–intensity diagram. The histogram represents the average count rate in the iron line in three flux intervals

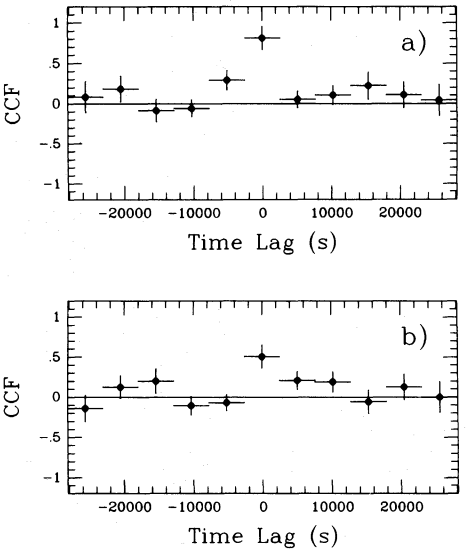


**Fig. 11a and b.** NGC 4051: **a** the cross correlation function between the light curves of the iron line and of the 3.5–5.8 keV continuum; **b** the cross correlation function between the light curves in the bands 3.5–5.8 and 8.1–18 keV. Each point represents the mean correlation in 5120 s

the variations in RC lag those in PC by more than three days in IC 4329A, by more than the duration of one *Ginga* orbit (90 min) and less than the duration of the observation in MCG-6-30-15 (but a much longer delay cannot be excluded), by less than 90 min in NGC 4051. In the case of MCG-6-30-15, under the assumption of a time lag formally zero (in practice less than the duration of one orbit), the hypothesis of changes in the slope of PC which are correlated with the intensity is equally acceptable as the previous one.

The iron line intensity is found to be variable in NGC 4051 at the 99% confidence level and to correlate with the continuum, in agreement with the conclusion above. In the other two objects it is consistent with a constant value: in IC 4329A it is not sufficiently well constrained for a consistency check with the above conclusion, in MCG-6-30-15 its behaviour is found to lend a marginally significant support to the hypothesis of a constant slope in PC.

The different behaviour of the three sources can be interpreted in terms of a difference in the size of the reprocessing region. According to the calculations by Matt et al. (1991), if the reprocessing gas is assumed to be in a flat accretion disk, then half of the reprocessed photons should come from within 40 to 80 gravitational radii ($r_g = GM/c^2$), depending on the disk inclination. The substantial difference in the time scale over which RC is found to vary in IC 4329A and NGC 4051 is therefore probably a consequence of the black hole mass being much larger in the first than in the second object. This conclusion is supported also by their different mean luminosity, $L_X = 10^{44}$ erg s$^{-1}$ for IC 4329A and $L_X = 2\,10^{41}$ erg s$^{-1}$ for NGC 4051.

(d) In IC 4329A and MCG-6-30-15 the spectra at low energies are well described by the two component model with a uniform absorber of constant density. This is not the case for NGC 4051, where further hypotheses are required. The two alternative hypotheses tested, namely a partial covering absorber and an uncovered soft component were both successful. In these two instances the effective $N_H$ appears to be inversely correlated with the source intensity, thus lending support to the case of a "warm absorber" in this galaxy; furthermore, changes occurring on time scale of the order of one day are implied either in the configuration of the absorber or in the intensity of the soft component.

*Acknowledgements.* We would like to thank all the members of the *Ginga* team for the support in data collection and in the data analysis system. The authors thank also R. Edelson and C. Done for useful discussions. F.F. wishes to thank the Japan Society for the Promotion of Science for his fellowship. G.C.P. acknowledges financial support from the Italian GIFCO/CNR and Ministry of University and Scientific Research (MURST).

## Appendix

The reliability of *Ginga* measurements of faint sources depends on systematic background subtraction errors. To minimize this effect useful data were selected according to the following conservative criteria:

(a) low particle induced background (surplus above upper discriminator (SUD) = count rate above 37 keV, less than 7.5 cts s$^{-1}$ det$^{-1}$);

(b) high geomagnetic cutoff rigidity (larger than 10 GeV/c);

(c) earth occultation angle greater than 7°.

We excluded also all the LAC data showing a correlation with those of the solid state electron monitor and those of the proportional counter and the scintillation counter of the *Ginga* gamma ray burst detector, which operates at 90° off the LAC direction.

The residual background includes contributions from several components as described in Hayashida et al. (1989);

(a) particle induced background;

(b) three radioactive features, with decay times of 5.5$^m$ 41$^m$ and 8 h, which arise from the exposure to the south atlantic anomaly (SAA) occurring on eight of the fifteen orbits each day;

(c) fluorescence lines, the strongest at 22.1 keV from the silver coating of the collimators;

(d) diffuse X-ray background (XRB).

An inaccurate estimate of the contribution of the latter component at the source position could give rise in principle to false spectral variations in faint sources because the XRB spectrum is flatter than that of a typical SG. However, Warwick & Stewart (1989) showed that the 2–10 keV slope of the spectrum of the XRB fluctuations is about 1.8, similar to that of a typical SG, and therefore the above effect should be negligible. False spectral variations could be produced also by an inaccurate evaluation of the internal background as a function of time, because the intensity and the spectrum of the first two components vary strongly with the position of the satellite. To minimize the latter error, row data should be accumulated with a fine time resolution and we chose to do so orbit by orbit both for the on- and the off-source observations.

Two independent methods were used for the background subtraction in the present analysis. The first is Method II in Hayashida et al. (1989). It has the advantage of reducing the effects of the XRB spatial fluctuations since the model background is obtained by utilizing a large number of blank field observations. The second takes advantage of background observations contiguous to the source, whose data are sorted according to the SUD level (e.g. MPYM). In the case of IC 4329A and NGC 4051, because the spectra of two distinct background pointings, before and after the source observation, were almost identical orbit by orbit, they were combined together. The two methods gave consistent results concerning the spectral shape, while the difference in the net count rate was always smaller than 0.7 cts s$^{-1}$. The results presented in this paper are those obtained with the second method.

Because of the complexity and the time variability of the *Ginga* background, there will always be a "systematic" uncertainty, regardless of the subtraction method adopted, which is important to evaluate. Hayashida et al. (1989) estimated the root mean square (RMS) of the residuals of the pulse height spectra after the background subtraction, with their methods I and II, by utilizing blank field observations lasting more than 1 day each. In this paper we are interested in the spectral variations of faint sources on time scales also much shorter than 1 day. For this reason and since two pairs of blank field pointings, made before and after the observations of IC 4329A and NCG 4051, were available, we computed the RMS of the residuals after the subtraction, orbit by orbit, of the spectra of the first observation of each pair from those of the second one. The resulting RMS of the counts in each energy channel for the two pairs of blank field observations were so similar that they were combined together. In Fig. 12 we show the RMS in cts s$^{-1}$ for seven detectors, obtained

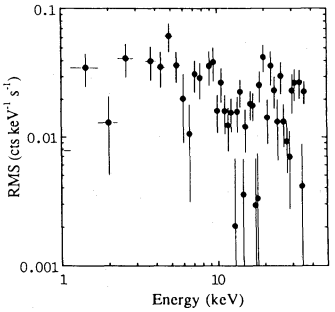


**Fig. 12.** Root mean squares, in cts $s^{-1}$ for seven detectors, of the residuals after subtracting, orbit by orbit, from the spectra accumulated observing a blank field, a background estimated using another blank field. The variance of purely statistical fluctuations has been subtracted channel by channel

after subtracting the variance of the Poisson statistical fluctuations, which should measure the magnitude of the systematic errors on time scale of about 1 orbit. RMS values in Fig. 12 are very similar to those in Figs. 13 and 14 of Hayashida et al. (1989) below 10 keV, but they are significantly greater at higher energies. In particular, a broad feature is quite evident at about 20 keV, which is probably due to small changes in the detector's gain which shifted the centroid of the line and produced, after the background subtraction, residuals around this energy. Above 18 keV the magnitude of the systematic errors is comparable to the count rate of two of the three sources. Therefore, for these sources, we used only the counts below 18 keV.

The systematic errors might have the same sign in contiguous channels and, therefore, they can increase when the counts are integrated in a band, thus introducing an artificial scatter in the colour diagrams. The values obtained in the extreme situation when they have the same sign in every channel of three bands 1.7–3.5, 3.5–5.8 and 8.1–18 keV, computed by summing up the RMS in Fig. 12, are 0.03, 0.1 and 0.15 cts $s^{-1}$, respectively. To evaluate the importance of the scatter introduced in the colour diagrams by this additional uncertainty, we considered the case of NGC 4051, the faintest source in our sample. Several thousands of intrinsically constant SC and HC were simulated with a total variance given by the sum of the variance of the statistical fluctuations and an extra term representing the variance due to the systematic errors. Each point was associated with an error bar representing the statistical fluctuations alone. Each point was associated with an error bar representing the statistical fluctuations alone. We then computed the $\chi^2$ distributions for the hypothesis of constant SC and HC. For the soft colour the $\chi^2$ distribution peaks at $\chi^2_r \sim 1.3$ and is not much different from that relative to the case of pure statistical fluctuations, thus indicating that even for a source as faint as NGC 4051 the systematic errors affects the SC values very little.

The situation for the hard colour is different, being the $\chi^2$ distribution for the constant hypothesis peaked at $\chi^2_r \sim 2.8$. As shown in Sect. 5, the $\chi^2_r$ for a constant HC in NGC 4051 is 2.0 and then the variance expected from the systematic errors given above is possibly greater than that actually measured. A still rather conservative estimate can, therefore, be obtained assuming that *all* the variance measured in the NGC 4051 HC is due to the systematic errors. These "fiducial" values correspond to about 65% of those given above.

## References


Bevington P.R., 1969, Data Reduction and Error Analysis for the Physical Science. McGraw-Hill, New York

Branduardi-Raymont G., 1986, in: Mason K.O., Watson M.G., White N. (eds.) The Physics of Accretion onto Compact Objects. Springer, Berlin, p. 407

Courvoisier T.J.-L., Camenzind M., 1989, A&A 224, 10

Disney M.J., 1973, ApJ 181, L55

Done C., Ward M.J., Fabian A.C., Kunieda H., Tsuruta S., Lawrence A., Smith M.G., Wamsteker W., 1990, MNRAS 243, 713

Edelson R., Krolik J., 1988, ApJ 333, 646

Fiore F., Perola G.C., Romano M., 1990, MNRAS 243, 552

Guilbert P.W., Rees M.J., 1988, MNRAS 233, 475

Halpern J.P., 1984, ApJ 281, 90

Hayashida K., et al., 1989, PASJ 41–3, 373

Kunieda H., Turner T.J., Awaki H., Koyama K., Mushotzky R., Tsuruta S., 1990, Nat 345, 786

Kunieda H., et al., 1991, ApJ (submitted)

Lampton M., Margon B., Bowyer S., 1976, ApJ 208, 177

Lawrence A., Watson M.G., Pounds K.A., Elvis M., 1985, MNRAS 217, 685 (LWPE)

Lightman A.P., White T.R., 1988, ApJ 335, 57

Makino F. & the ASTRO-C team 1987, Astron. Lett. Commun. 25, 223

Matt G., Perola G.C., Piro L., 1991, A&A 247, 25

Matsuoka M., Piro L., Yamauchi M., Murakami T., 1990, ApJ 361, 440 (MPYM)

Morrison R., McCommon D., 1983, ApJ 270, 119

Nandra K., Pounds K.A., Stewart G.C., Fabian A.C., Rees M.J., 1989, MNRAS 236, 39

Nandra K., Pounds K.A., Stewart G.C., 1990, MNRAS 242, 660 (NPS)

Nandra K., Pounds K.A., Stewart G.C., George I.M., Hayashida K., Makino F., Ohashi T., 1991, MNRAS 248, 760

Pan H.C., Stewart G.C., Pounds K.A., 1990, MNRAS 242, 177

Perola G.C., Altamore A., Bromage G.E., Boksenberg A., Clavel J., Elvius A., Fiore F., Penston M.V., Piro L., Snijders M.A.J., Ulrich M.A., 1986, ApJ 306, 508

Piro L., Yamauchi M., Matsuoka M., 1990, ApJ 360, L35

Pounds K.A., Turner T.J., Warwick R.S. 1986, MNRAS 221, 7

Pounds K.A., Nandra K., Steward G.C., George I.M., Fabian A.C., 1990, Nat 344, 132

Turner T.J., 1987, MNRAS 232, 463

Turner M.J.L., et al., 1989, PASJ 41–3, 345

Walter R., Courvoisier T.J.-L., 1990, A&A 233, 40

Warwick R.S., Stewart G.C., 1989, in: Hunt J., Battrick B. (eds.) Proc. 23rd ESLAB Symp. ESA SP-296, Vol. 2, p. 727

White T.R., Lightman A.P., Zdziarski A.A., 1988, ApJ 331, 939

Yaqoob T., Warwick R.S., 1991, MNRAS 248, 773

Yaqoob T., Warwick R.S., Pounds K.A., 1989, MNRAS 236, 153